

# Viscous dynamics of drops and bubbles in Hele-Shaw cells: drainage, drag friction, coalescence, and bursting

Ko Okumura (okumura.ko@ocha.ac.jp)

*Physics Department, Faculty of Science, Ochanomizu University*

## Abstract

In this review article, we discuss recent studies on drops and bubbles in Hele-Shaw cells, focusing on how scaling laws exhibit crossovers from the three-dimensional counterparts and focusing on topics in which viscosity plays an important role. By virtue of progresses in analytical theory and high-speed imaging, dynamics of drops and bubbles have actively been studied with the aid of scaling arguments. However, compared with three dimensional problems, studies on the corresponding problems in Hele-Shaw cells are still limited. This review demonstrates that the effect of confinement in the Hele-Shaw cell introduces new physics allowing different scaling regimes to appear. For this purpose, we discuss various examples that are potentially important for industrial applications handling drops and bubbles in confined spaces by showing agreement between experiments and scaling theories. As a result, this review provides a collection of problems in hydrodynamics that may be analytically solved or that may be worth studying numerically in the near future.

Keywords: drops and bubbles; Hele-Shaw cell; scaling laws; viscous dynamics; thin film

## Contents

I. Introduction	2
II. Life time of a bubble	3
III. Drag friction acting on a bubble	4
IV. Drag friction acting on a liquid drop	6
V. Non-linear viscous drag friction	8
VI. Drop Coalescence	10
VII. Film bursting in a Hele-Shaw cell	14
VIII. Conclusion	15
Acknowledgments	15
References	16

## I. INTRODUCTION

When a bubble is injected in a glass of milk, the bubble rises up in the liquid and comes up at the liquid-air interface making a hemispherical air bubble encapsulated by a film of the liquid. The bubble stays at the interface with keeping the hemispherical shape but with decreasing the thickness of the liquid film due to drainage. After some waiting time, a hole is created and grows in the thin film, which leads to disappearance of the bubble. Similar processes are observed with a highly viscous liquid even with lavas during volcanic eruptions and even in the absence of surfactants.

These simple phenomena familiar to everyone involve several elementary processes, such as creation of a bubble, rising of a bubble, film drainage, nucleation of a hole, and bursting of a thin film. We will explore these phenomena and how dynamics change when the bubble is confined in between two plates of a Hele-Shaw cell. Throughout this review, we limit ourselves to the case in which there are no effects of surfactants. We also discuss the case

in which the air bubble is replaced with a fluid drop and the case of coalescence of a drop with a bath of the same liquid in a Hele-Shaw cell.

For the readers' convenience, we here introduce some notations used in this review although they are re-introduced in the main text below as we proceed:

- $\eta_1$  and  $\rho_1$ : viscosity and density of a fluid drop (a bubble or a liquid drop).
- $\eta_2$  and  $\rho_2$ : viscosity and density of another fluid (liquid or air) surrounding the fluid drop.
- $\Delta\rho = |\rho_1 - \rho_2| > 0$  the density difference of the two fluids; in discussing a bubble this is practically equal to the density of the surrounding fluid  $\rho_2$ .
- $\gamma_{12}$  interfacial energy between the fluid drop and the surrounding fluid; in discussing a bubble, this is equal to the surface tension of the surrounding fluid  $\gamma_2$  (in discussing a liquid drop in air in Sec.VI, this is equal to the surface tension of the liquid drop  $\gamma_1$ ).
- $\kappa_{12}^{-1} = \sqrt{\gamma_{12}/(\Delta\rho g)}$  capillary length for the interface between the fluid drop and the surrounding liquid; in discussing a bubble, this is practically equal to the capillary length for the surrounding fluid  $\kappa_2^{-1} = \sqrt{\gamma_2/(\rho_2 g)}$

## II. LIFE TIME OF A BUBBLE

When a bubble is created in a ultra-viscous liquid (viscosity  $\eta_2$  and density  $\rho_2$ ), it raises up to make a hemispherical bubble at the liquid-air interface as shown in Fig. 1, and stays there for a considerably long time, even though there are no effects of surfactants, before it breaks up by bursting of the spherical thin film encapsulating the bubble. In such a case, the life time of the bubble is governed by the drainage of liquid from the thin film. With taking the  $\theta$  coordinate as the angle from the bubble top along the bubble surface ( $\theta = 0$  at the top and  $\theta \simeq \pi/2$  at the liquid-air interface), the thinning dynamics of the film of thickness  $h$  is known [1] to be given by

$$h = h_0 f(\theta) e^{-t/\tau} \quad (1)$$

for the initial thickness  $h_0$  at the top of the bubble, i.e., at  $\theta = 0$ , with the life time  $\tau$  and the function  $f$  given by

$$\tau = \eta_2/(\rho_2 g R) \quad (2)$$

$$f(\theta) = 1/\cos^4(\theta/2) \quad (3)$$

with the radius of the bubble  $R$  and the gravitational acceleration  $g$ .

This scaling law for the life time can be understood as follows. In the present case, the velocity  $\mathbf{v}$  satisfies the following lubricant equation:

$$\eta_2 \nabla^2 \mathbf{v} = -\rho_2 \mathbf{g}, \quad (4)$$

where  $\mathbf{v} = v(\theta)\mathbf{e}_\theta$  with  $\mathbf{e}_\theta$  the unit vector in the  $\theta$  direction and the gravitational acceleration vector  $\mathbf{g}$  pointing in the direction  $\theta = \pi$ . This equation can be solved in the form  $v(\theta) \simeq (\rho_2 g R^2/\eta_2) \sin \theta$ , which results from the fact that the flow is a plug flow and does not change in the direction of the film thickness (i.e., the direction of the  $r$  coordinate for which  $r = R$  at the bubble surface). The conservation equation,

$$\frac{\partial h}{\partial t} + \nabla \cdot (h\mathbf{v}) = 0, \quad (5)$$

can be solved through a separation of variables, which gives Eq. (1) with Eqs. (2) and (3), by noting that  $h = h(t, \theta)$  and  $\nabla \cdot (h\mathbf{v}) = \partial(\sin \theta h v)/\partial \theta/(R \sin \theta)$ .

When a bubble is sandwiched by two cell plates separated by the distance  $D$  in a Hele-Shaw cell, the boundary condition changes as illustrated in Fig. 2. Because of this, Eq. (1) gives  $v(\theta) \simeq (\rho_2 g D^2/\eta_2) \sin \theta$  for  $D < R$ . In addition, the divergence appearing in the conservation equation is changed into  $\nabla \cdot (h\mathbf{v}) = \partial(hv)/\partial \theta/R$ . As a result, Eqs. (2) and (3) are replaced by

$$\tau = 12\eta_2 R/(\rho_2 g D^2) \quad (6)$$

$$f(\theta) = 1/\cos^2(\theta/2) \quad (7)$$

for  $D < R$ . This theory is confirmed well in Ref. [2].

### III. DRAG FRICTION ACTING ON A BUBBLE

When a bubble is created in a liquid bath (viscosity  $\eta_2$  and density  $\rho_2$ ), the bubble rises up in the liquid. When the rising velocity  $V$  is small, we can assume that the shape of the

rising bubble is practically a spherical shape of radius  $R$ . In such a case, the drag friction acting on the bubble is given by

$$F \simeq \eta_2 V R, \quad (8)$$

Note that Stokes' friction law for a solid sphere with radius  $R$  moving with a velocity  $V$  in a viscous liquid with viscosity  $\eta$  is given by  $F = 6\pi\eta VR$ .

When a bubble is sandwiched by the two cell walls separated by the distance  $D$  of a Hele-Shaw cell, the drag force is found [3] to be given by

$$F \simeq \eta_2 V R_T^2 / D \quad (9)$$

The experimental set up to confirm this is shown in Fig. 3(a), together with a related set up discussed later. The air drop is slightly elongated, which is characterized by the transverse and longitudinal lengths  $R_T$  and  $R_L$  as defined in Fig. 4(a).

The scaling law given in Eq. (9) is explained by considering the slight deformation of the bubble shape. When viscous dissipation is dominant for the velocity gradient  $V/D$  developed near the bubble between the cell plates separated by  $D$ , the balance between the viscous dissipation and gravitational energy gain (per unit time) can be expressed as

$$\eta_2 (V/D)^2 R_T^2 D \simeq \rho_2 g R_T R_L D V. \quad (10)$$

This results in

$$V \simeq (R_L/R_T) \rho_2 g D^2 / \eta_2, \quad (11)$$

which is discussed in [4] and [5] as further explained below. If Eq. (10) is expressed in the force-balance form  $\eta_2 V R_T^2 / D \simeq \rho_2 g R_T R_L D$ , we immediately know that the drag friction acting on the bubble from the viscous medium is given by Eq. (9).

In order to observe this scaling law, dissipation associated with the velocity gradient  $V/D$  wins over other viscous dissipations, such as those associated with velocity gradient  $V/R_T$ , and  $V/R_L$ , from which the condition  $D < R_T, R_L$  is required. An important fact to be noted here is that in the present experiment, since the liquid surrounding the bubble completely wet the cell plates, there are thin layers of the liquid between the cell plates and both surfaces of the disk-shaped bubble (see the left side view in Fig. 3). The creation of velocity gradient  $\simeq V/h$  with  $h$  the thickness of layers is energetically unfavorable due to the relation  $h \ll D$ , and because of this the dissipation associated with the gradient  $V/D$

becomes dominant in the present case. However, this is not always the case, as shown in Sec. V.

The scaling law in Eq. (9) is confirmed in Fig. 5. In (a), the rising velocity  $V$  is given as a function of the cell thickness  $D$  for different parameters,  $R_T$ ,  $R_L$ , and  $\nu_2 = \eta_2/\rho_2$ . In (b), the same data are plotted with renormalized axes, on the basis of the dimensionless form of Eq. (9),  $(R_T/R_L)Ca = D/\kappa_2^{-1}$ , with the capillary number  $Ca = \eta_2 V/\gamma_2$  and the capillary length  $\kappa_2^{-1} = (\gamma_2/(\rho_2 g))^{1/2}$ , to show a clear data collapse, confirming the validity of Eq. (9). Although the values of the factor  $R_T/R_L$  for the data used in Fig. 5 are relatively close to one, this factor is important for the clear data collapse; it is confirmed in [3] that if this factor is set to one the quality of the collapse is clearly deteriorated.

The rising bubble in a Hele-Shaw cell discussed above was theoretically studied by Taylor and Saffman [4] (earlier than the Bretherton's paper on bubbles in tubes [6, 7]) and by Tanveer [5]. Other theoretical works on fluid drops in the Hele-Shaw cell geometry includes the topological transition associated with droplet breakup [8–11].

Experimentally, a number of researchers have investigated the rising motion of a bubble in a Hele-Shaw cell [12–15], together with studies performed in different geometries, which includes studies on inertial regimes (Crossovers between viscous regimes treated in this review and inertial and other regimes are fruitful future challenges) [16–18]. However, they have mostly concerned with the case in which there is a forced flow in the outer fluid phase and/or the case in which the cell is strongly inclined nearly to a horizontal position.

One of the features of the present case is that thin liquid films surrounding a bubble plays a crucial role as mentioned above (see the left side view in Fig. 3): in many previous works, the existence of such thin films is not considered. In this respect, the present problem is closely related to the dynamics governed by thin film dissipation such as the imbibition of textured surfaces [19–24], as further discussed in Sec. V. In this sense, our problem is quasi two-dimensional, although the geometry of the Hele-Shaw cell is often associated with a purely two-dimensional problem.

#### IV. DRAG FRICTION ACTING ON A LIQUID DROP

Even if an air bubble is replaced by a liquid drop (density  $\rho_1$ ) whose viscosity  $\eta_1$  is smaller than that of the surrounding bath liquid  $\eta_2$ , the drag friction and the cor-

responding velocity are still given respectively by Eqs. (9) and (11):  $F \simeq \eta_2 V R_T^2 / D$  and  $V \simeq (R_L / R_T) \Delta \rho g D^2 / \eta_2$ . Note that, in the second equation,  $\rho_2$  is replaced with  $\Delta \rho = |\rho_2 - \rho_1|$ , which is practically equal to  $\rho_2$  in the previous section with a bubble of density  $\rho_1$ .

The experimental setup for confirming this law is illustrated in Fig. 3(b). In this case, the fluid drop goes down, because the density of the drop is larger than that of the surrounding drop, and the drop shape is considerably similar to that of an air bubble, as shown in Fig. 4(b).

However, when the drop viscosity  $\eta_1$  is larger than that of the surrounding liquid  $\eta_2$  as in Fig. 4(c), the drag friction is found to be given by the following scaling law [3]:  $F \simeq \eta_1 V R_T R_L / D$ . This scaling law is expected because the Eq. (10) is replaced by  $\eta_1 (V/D)^2 R_T R_L D \simeq \Delta \rho g R_T R_L D V$ . In this case, the shape of the drop is significantly elongated compared with the previous case.

In summary, two scaling regimes of the viscous drag friction acting on a fluid drop in a Hele-Shaw cell ( $R_L, R_T > D$ ) are identified as follows:

$$F \simeq \begin{cases} (R_L / R_T) \Delta \rho g D^2 / \eta_2 & \eta_2 \gg \eta_1 \\ \eta_1 V R_T R_L / D & \eta_2 < \eta_1 \end{cases} \quad (12)$$

with the corresponding velocity laws:

$$V \simeq \begin{cases} (R_L / R_T) \Delta \rho g D^2 / \eta_2 & \eta_2 \gg \eta_1 \\ \Delta \rho g D^2 / \eta_1 & \eta_2 < \eta_1 \end{cases} \quad (13)$$

The crucial condition for these scaling laws to appear is that the formation of thin layers of the surrounding liquid between the cell plates and both surfaces of the disk-shaped droplet (see the right side view in Fig. 3). Otherwise, the drop would directly contact with the cell plates making contact lines, and the dynamics would be affected by the contact angle hysteresis (CAH). In general, physical understanding of CAH is very limited and CAH is sensitive to even a slight contamination of the surface. Thus, if a special care is properly taken for the surface of cell walls, the study of drag friction under the existence of the contact line would be a challenging future problem.

It is worth mentioning that in the three dimensional case, in the limit of highly viscous fluid drop,  $\eta_2 \ll \eta_1$ , which corresponds to the viscous friction acting on a solid sphere, is given by Eq. (8), in which  $\eta_1$  is absent in contrast with Eq. (12). This is again because

of the existence of the thin layers of the surrounding fluid whose thickness is  $h$ . However, when  $\eta_1$  is extremely larger than  $\eta_2$ , depending on the thickness of the layers, dissipation associated with the viscous stress  $\eta_2 V/h$  becomes smaller than that with  $\eta_1 V/D$ . This case is discussed in Sec. V.

In Fig. 6, Eq. (13) for  $\eta_2 < \eta_1$  is directly confirmed, and thus Eq. (12) for  $\eta_2 < \eta_1$  are indirectly confirmed, for the data represented by the filled symbols. However, the data represented by open symbols do not follow the scaling law, which is the case mentioned in the previous paragraph and discussed in the next section. Note that (as clear from theoretical arguments above) Eqs. (12) and (13) for  $\eta_2 > \eta_1$  are physically the same as Eqs. (9) and (11), respectively, which is shown experimentally in [3].

## V. NON-LINEAR VISCOUS DRAG FRICTION

When the dissipation in the thin film is dominant, the velocity law is given by

$$\eta_2 V \simeq \gamma_{12} (D/\kappa_{12}^{-1})^3 \quad \text{for } D > \kappa_{12}^{-1} \quad (14)$$

and corresponding friction law is non-linear in  $V$ :

$$F \simeq (\eta_2 V/\gamma_{12})^{1/3} \gamma_{12} R_T R_L / \kappa_{12}^{-1} \quad \text{for } D > \kappa_{12}^{-1} \quad (15)$$

with the capillary length  $\kappa_{12}^{-1} = \sqrt{\gamma_{12}/\Delta\rho g}$  defined for the drop-bath interface whose interfacial energy is  $\gamma_{12}$ . For  $D < \kappa_{12}^{-1}$ , the velocity and force are replaced by the following expressions, respectively:  $\eta_2 V \simeq \gamma_{12} (D/\kappa_{12}^{-1})^6$  and  $F \simeq (\eta_2 V/\gamma_{12})^{1/3} \gamma_{12} R_T R_L / D$ . We note here that the viscous friction forces including this nonlinear friction and that given in Eq. (15) are relevant to the dynamics of emulsion, foam, antifoam and soft gels [25–27], in particular, nonlinear rheology of such systems [28–30].

Equations (14) and (15) are derived because Eq. (10) is replaced with

$$\eta_2 (V/h)^2 R_T R_L h \simeq \Delta\rho g R_T R_L D V, \quad (16)$$

with  $h$  the thickness of the thin layers of the surrounding liquid, and because, on the basis of the scaling arguments, [31] the thickness of the film is expected to be given by

$$h = k \kappa_{12}^{-1} (\eta_2 V/\gamma_{DB})^{2/3} \quad (17)$$



The value numerical coefficient  $k$  is estimated as 0.94 in a more rigorous calculation in Refs. [32, 33]. With Eq. (14), Eq. (17) can be expressed as

$$h \simeq \kappa_{12}^{-1} (D/\kappa_{12}^{-1})^2 \quad \text{for } D > \kappa_{12}^{-1} \quad (18)$$

For  $D < \kappa_{12}^{-1}$ , the thickness is given by the expression [34]  $h \simeq D(\eta_2 V/\gamma_{12})^{2/3} \simeq D(D/\kappa_{12}^{-1})^4$ , which leads to the above-mentioned velocity and drag force for  $D < \kappa_{12}^{-1}$ .

The scaling law in Eq. (14) is directly confirmed, and thus Eq. (15) is indirectly confirmed, in Fig. 7(a), as explained in the caption. The data used in Fig. 7(a) are the ones plotted in Fig. 6 in a different way by using the same open symbols. In Fig. 6, these data are not on the dashed line but on horizontal lines; instead, the data with the same value of  $D$  are on the same horizontal line. This is consistent with Eq. (14) because  $\eta_2$ ,  $\gamma_{12}$ , and  $\kappa_{12}^{-1}$  are approximately fixed for the data, and in such a case the value of  $\eta_2 V$  is classified by the value of  $D$ .

The condition for the crossover between linear and non-linear viscous frictions, corresponding to that between Eq. (13) for  $\eta_2 < \eta_1$  and Eq. (14), can be determined by comparing the magnitude of dissipations of the two regimes:  $\eta_1 (V/D)^2 R_T R_L D \simeq \eta_2 (V/h)^2 R_T R_L h$ . This condition can be written as

$$\eta_2/\eta_1 \simeq D/\kappa_{12}^{-1} \quad (19)$$

This condition is confirmed in Fig. 7(b), as explained in the caption, by using the data in Fig. 6. From this phase diagram, we expect, for example, the crossover between the two regimes for the series of data obtained for  $D \simeq 1$  mm (red symbols). This crossover can be directly confirmed in Fig. 6. The left three red (open) symbols are on the horizontal line, whereas right two red (filled) symbols are on the dashed line. Note that red filled circles and red filled inverse triangles are exceptional data: these data are obtained when droplets go down nearly on the same trail more than once; as a result, mixing of the two liquids comes into play, which increases the viscosity of the thin layers sandwiched between the bubble and cell plates and makes the velocity gradient in the thin films unfavorable (see Ref. [35] for the details).

Knowing that there are different scaling regimes for viscous drag friction in the Hele-Shaw cell, a natural question to ask would be how the friction law will change if the surrounding fluids are replaced with granular particles in the cell. Such a study was performed by using the setup shown in Fig. 8. The cell filled with granular particles (diameter  $d$  and density

$\rho$ ) can be moved at a constant velocity  $V$  and the drag force  $F$  acting on the obstacle of radius  $R$  can be monitored by the force gauge by virtue of a non-extensible strong fishing line connecting the obstacle and the force gauge. As a result, the drag force  $F$  is found [36, 37] to be given (1) by the dynamic part scaling as  $V^2$  governed by the momentum transfer associated with collisions between the obstacle and cluster of grains ahead of it and (2) by the static part  $F_0$  governed by the friction force (friction coefficient  $\mu$ ) acting on the cluster from the bottom plate of the cell:

$$F - F_0 \simeq \rho(\phi_c - \phi)^{-1/2} R^3 V^2 / d \quad (20)$$

$$F_0 \simeq \mu \rho g R^2 (\phi_c - \phi)^{-1/2} d \quad (21)$$

where  $\phi$  is the packing fraction and  $\phi_c$  is a critical density at which the drag force diverges. This divergence, related to dynamic jamming of grains ahead of the obstacle [38, 39], is clearly confirmed in Fig. 9. Interestingly, the value of  $\phi_c \simeq 0.841$  obtained from the experiment exactly matches the static jamming point in two dimension [40, 41]. The background of this study is briefly summarized as follows. The dynamic jamming has actively been explored [42–45]. Experiments on soft colloids [29, 30] have demonstrated good agreements with a phenomenological theory [46]. However, as for granular systems, simulations and a scaling phenomenology revealed critical behaviors different from those of soft colloids [47–49]. Experimentally, at high velocities ( $\gtrsim 100$  mm/s) and high densities, a force component scaling with velocity squared has been reported through impact experiments [50–52], while different velocity dependences have been reported in particular at much slower velocities [53–61]. The divergence of the drag force at high velocities discussed above has been examined in recent numerical studies [62, 63].

## VI. DROP COALESCENCE

When a rain drop falling on the surface of a puddle, the rain drop coalesces into the puddle. This is because the area of the liquid-air interface is made smaller by the process. Figure 10(a) shows a series of snapshots of such a coalescence, but with minimizing the "falling velocity": the coalescence is here initiated by touching the two droplets that are held at the tips of pipets with a speed negligible for the coalescence dynamics [64]. From

the figure, we see the formation of a neck between the tips of the droplets that grows with time  $t$ .

Theoretical prediction was made analytically by Eggers and co-workers in 1999 [65], and here we reproduce the result at the level of scaling laws. The driving force is surface tension, which is opposed by inertial and viscous forces. We estimate changes of the corresponding three energies per unit time. The change of surface energy,  $dE_c/dt \simeq d(\gamma_1 r^2)/dt \simeq \gamma_{12} r^2/t$ , with the neck size  $r$  and the surface energy (per unit area)  $\gamma_1$ , which can be expressed as  $\gamma_{12}$  (the interfacial energy between the drop and the surrounding fluid, i.e., air). This is because when a neck with radius  $r$  is formed, the total area the two droplets is decreased by an amount of order of  $r^2$ . This energy will be lost by viscous dissipation and/or changed into kinetic energy.

In the small  $r$  limit, viscous dissipation dominates because the volume of moving region is small. In such a case, the two droplets contact with each other nearly by a point, implying that there is only a single length scale for the moving region, which is  $r$ . As a result, viscous dissipation per time is given as  $dE_v/dt \simeq \eta_1 (V/r)^2 r^3$ , where  $\eta_1$  is viscosity of the liquid drop and  $V \simeq r/t$  is the growth rate of the neck size. This is because viscous dissipation per unit time and per unit volume scales as  $\eta_1 (V/r)^2$  and the volume of dissipation scales as  $r^3$ .

When  $r$  gets larger, kinetic energy comes into play. Since the length of neck scales as  $r^2/R$  from a geometrical consideration, kinetic-energy increase per unit time scales as  $dE_i/dt \simeq \rho_1 r^2 (r^2/R) V^2/t$ .

From the above arguments, at short times surface energy is lost in viscous dissipation:  $dE_c/dt \simeq dE_v/dt$ , that is,  $r \simeq \gamma_{12} t / \eta_1$ . In fact, Eggers and co-workers predicted an extra correction term proportional to  $\log t$ , which has not been confirmed experimentally. In the same way, at later times, surface energy is changed into kinetic energy:  $dE_c/dt \simeq dE_i/dt$ , that is,  $r \simeq (\gamma_{12} R / \rho_1)^{1/4} t^{1/2}$ . The two scaling relations, one for the initial viscous regime and another for the later inertial regime can be expressed in the following dimensionless forms:

$$r/R \simeq \begin{cases} t/\tau_v & \text{for viscous regime } (t < \tau) \\ (t/\tau_i)^{1/2} & \text{for inertial regime } (t > \tau) \end{cases} \quad (22)$$

with  $\tau_v = \eta_1 R / \gamma_{12}$ ,  $\tau_i = (\rho_1 R^3 / \gamma_{12})^{1/2}$ , and  $\tau = \tau_v^2 / \tau_i$ .

An example of experimental confirmation of Eq. (22) is given in Fig. 10(b) and (c), in which  $r$  and  $R$  are replaced with  $R$  and  $R_0$ , respectively. The top plots in (b) and (c) show

the raw data in the two regimes. The bottom plots show that the data are well collapsed onto the master curves by rescaling of the axes, which confirms Eq. (22).

The crossover between the two regimes in Eq. (22) is experimentally confirmed in Fig. 11 [66], in which  $(r, \gamma_{12}, \eta_1, \rho_1, t)$  is replaced with  $(r_{\min}, S, \eta_0, \rho_0, \tau)$ . Here, this crossover is confirmed in a different system. When a liquid drop of dodecane is placed on the surface of bath water, the drop takes a thin lens shape. The coalescence of two of such floating droplets are captured in Fig. 11(a). In this geometry, the coalescence is found to be purely two-dimensional, meaning that the velocity gradient in the direction of the thickness of the lens is practically negligible, for which Eq. (22) is valid. As a result, a clear scaling crossover of the coalescence dynamics is shown in Fig. 11(b). Note that various crossovers of scaling regimes for a coalescence of a fluid drop surrounded by another fluid in three-dimension are recently discussed [67].

Figure 12 shows an experimental setup to observe drop coalescence in a Hele-Shaw cell [68]. The cell is held in the upright position. First, the cell is half-filled by polydimethylsiloxane (PDMS). Second, a glycerol aqueous solution is poured into the cell. Then, the heavier glycerol solution replaces the lower PDMS phase. This replacement leaves thin layers of PDMS in the lower phase, which are sandwiched by the bottom glycerol phase and the cell plates (see the side view in Fig. 12). This is because the acrylic plates are completely wetted by the oil. After the formation of two phases, a droplet of the glycerol solution is created in the upper oil phase, which slowly goes down the oil phase to touch the oil-glycerol interface, at which coalescence of the droplet and liquid bath of the same liquid is initiated.

Figure 13 shows snapshots at short times (initial stage) and those at large times (final stage). These photographs are obtained by a high-speed camera. The time interval between adjacent shots in Fig. 13(b) are ten times larger than that in Fig. 13(a), indicating the dynamics slows down significantly at large times.

Figure 14 shows two scaling regimes characterized by slope 1 (i.e., the neck size  $r$  scales with  $t$  at short times) and slope  $1/4$  (i.e., the neck size  $r$  scales with  $t^{1/4}$  at large times), which helps us to construct a theory. Before this, let us remark on experimental tricks introduced in the present experiment. In this experiment, as explained in the second paragraph above in which Fig. 12 is first mentioned, the oil phase is deliberately introduced to remove the effect of contact line, which is difficult to control: since the liquid disk is sandwiched by thin layers of the oil, the disk has no direct contact with the cell walls. In addition, the viscosity

of oil  $\eta_2$  is set to much smaller than that of the glycerol solution  $\eta_1$ : the oil phase could play the role of air phase in the three-dimensional counterpart.

Considering these points, we see that the dynamics of the initial regime could be the same as the three-dimensional initial dynamics, which is characterized by the slope 1. This is because at short times when  $r$  is much smaller than the cell thickness  $D$  the dynamics could become independent of the existence of the cell walls: the effect of confinement by the cell walls is practically negligible.

On the contrary, the dynamics at the final stage characterized by slope 1/4 reflects the effect of confinement of wall as discussed below. In the present confined case, we have good reasons to make the following replacements from the three-dimensional viscous counterpart: (1) The gain in surface energy per unit time should be changed from  $dE_c/dt \simeq d(\gamma_{12}r^2)/dt$  to  $dE_c/dt \simeq d(\gamma_{12}rD)/dt$ . (2) The viscous dissipation per unit time should be changed from  $dE_v/dt \simeq \eta_1(V/r)^2r^3$  to  $dE_v/dt \simeq \eta_1(V/D)^2rDd$  where  $d$  is the height of the neck, with which the volume of the neck is expressed as  $rDd$ . The first replacement is rather obvious because the three-dimensional circular shape of the area  $\simeq r^2$  that disappears as a result of coalescence is here confined by the wall to take a quasi-rectangular shape of area  $\simeq rD$ . The second replacement is expected as long as  $d \gtrsim D$ , in which case the dominant viscous dissipation per unit time and unit volume scales as  $\eta_1(V/D)^2$  is localized in the neck volume  $\simeq rDd$ . In addition, from a geometrical relation,  $R^2 = (R - d)^2 + r^2$ , the neck height  $d$  is expressed as  $d \simeq r^2/R$  as long as  $R \gtrsim d$ . By balancing the capillary energy gain with the viscous dissipation thus justified, we obtain  $r \simeq (\gamma_{12}RD^2t/\eta_1)^{1/4}$ , which leads to the desired slope 1/4.

In summary, the dynamics exhibits a dimensional crossover from the short-time three-dimensional one to the long-time quasi-two-dimensional one, expressed by the following set of equations, which are confirmed in Fig. 15.

$$r/D \simeq t/\tau_I \quad \text{for } r < D \quad (23)$$

$$r/\sqrt{RD} \simeq (t/\tau_F)^{1/4} \quad \text{for } \sqrt{RD} < r < R \quad (24)$$

with  $\tau_I = \eta_1 D/\gamma_{12}$ , and  $\tau_F = \eta_1 R/\gamma_{12}$ . Some remarks are as follows. (1) Equation (23) is another dimensionless form of the viscous regime given in Eq. (22). (2) The condition,  $\sqrt{RD} < r < R$ , for the final regime to be valid implies that this dynamics is well observed

when  $D \ll R$  is satisfied, which is true for the experimental data. (3) The final regime is predicted to start from  $r$  and  $t$  are larger than  $\sqrt{RD}$  and  $\tau_F$ , respectively, which are well confirmed in Fig. 15(b).

There are a number of future problems for the quasi-two-dimensional coalescence. One is to find an inertial regime since only viscous regimes have been found. In the three-dimensional liquid drop coalescence in air, the Ohnesorg number ( $Oh \simeq \eta_1/\sqrt{\rho_1\gamma_1 R}$ ) appears when we discuss the crossover between the viscous and inertial regimes given in Eq. (22): we can express the crossover by the simple expression  $r/R = Oh$ . In the quasi-two dimensional case, the corresponding number will be useful to look for different regimes including inertial regimes. Another interesting problem would be to find partial coalescence in the quasi-two-dimensional case, which has been discussed for a number of systems in three dimension [69–71].

## VII. FILM BURSTING IN A HELE-SHAW CELL

When the coalescence experiment is performed with a different combination of liquids, glycerol solution and olive oil, the mode of coalescence significantly changes as shown in Fig. 16, because thin film (viscosity  $\eta_2$ ) formed between the drop and bath of the same liquid (viscosity  $\eta_1$ ) is more stable in the present case (molecules contained in olive oil may play a role similar to surfactants). This problem can be seen as a problem of film bursting.

Bursting of liquid thin film is familiar to everybody as the rupture of soap films, and is important in many fields [72–74]. Although the fundamental physics of the dynamics of bursting film is rather well and simply understood [31], in all previous studies the bursting hole has circular symmetry, which is lost in the present case. Here, the problem is bursting of a thin film in a confined geometry, which is relevant in many practical situations where small amount of liquids has to be manipulated (e.g., microfluidics and biological applications).

When the circular symmetry is preserved, the bursting or dewetting frequently proceeds with a constant speed and in such cases a rim is formed as in the bursting of soap film in air [75–77] or in the surrounding oil phase [78] and in the bursting of liquid film on a solid substrate (i.e. dewetting) [79]; when the rim is not formed the speed grows exponentially as observed in the bursting of highly viscous films suspended in air [1, 80].

On the contrary, when the circular symmetry is lost, the bursting proceeds with a constant

speed but no rim is formed and the velocity  $V$  is found [81] to be a constant given by

$$V \simeq \gamma_{12}/\eta_1 \quad (25)$$

when  $\eta_1 \gtrsim \eta_2$ . This scaling law can be derived by the balance of energy per unit time:

$$\gamma_{12}DV \simeq \eta_1(V/h)^2 h^2 D \quad (26)$$

This scaling regime is significantly different from the three-dimensional case because the dynamics proceeds with a constant speed although the rim is not formed.

## VIII. CONCLUSION

In this review, we discussed viscous dynamics of bubbles in Hele-Shaw cells, focusing on drainage and drag friction. We further explored the problem of drag friction in a Hele-Shaw cell when the bubble is replaced by a viscous drop or the surrounding liquid is replaced by granular medium to demonstrate examples of nonlinear friction dynamics. In addition, viscous coalescence of a liquid drop with a bath of the same liquid is also discussed, together with film bursting problems. The collection of examples provided in this review is not exhaustive but enough to show that the effects of confinement provided by Hele-Shaw cells are worth studying further in the near future. The scaling laws that emerge from these examples are relevant for industrial applications dealing with drops and bubbles in confined spaces such as petroleum industry [15] and microfluidic applications [82], as well as for industrial and fundamental problems associated with foams and microemulsions [25, 83]. The scaling laws in the Hele-Shaw geometry discussed here have been established only by agreement between experiments and scaling phenomenologies, providing future challenges for analytical and numerical studies.

## Acknowledgments

This work was partly supported by Grant-in-Aid for Scientific Research (A) (No. 24244066) of JSPS, Japan, and by ImPACT Program of Council for Science, Technology

and Innovation (Cabinet Office, Government of Japan).

---

- [1] Debrégeas, G., de Gennes, P.-G. & Brochard-Wyart, F. The life and death of "bare" viscous bubbles. *Science* **279**, 1704–1707 (1998).
- [2] Eri, A. & Okumura, K. Lifetime of a two-dimensional air bubble. *Phys. Rev. E* **76**, 060601(R) (2007).
- [3] Eri, A. & Okumura, K. Viscous drag friction acting on a fluid drop confined in between two plates confined in between two plates. *Soft Matter* **7**, 5648 (2011).
- [4] Taylor, G. & Saffman, P. G. A note on the motion of bubbles in a hele-shaw cell and porous medium. *Quarterly J. Mech. Applied Math.* **12**, 265–279 (1959).
- [5] Tanveer, S. The effect of surface tension on the shape of a hele-shaw cell bubble. *Phys. Fluids* **29**, 3537–3548 (1986).
- [6] Bretherton, F. P. The motion of long bubbles in tubes. *J. Fluid. Mech.* **10**, 166 (1961).
- [7] Clanet, C., Héraud, P. & Searby, G. On the motion of bubbles in vertical tubes of arbitrary cross-sections: Some complements to the dimitrescu-taylor problem. *J. Fluid Mech.* **519**, 359–376 (2004).
- [8] Eggers, J. Nonlinear dynamics and breakup of free-surface flows. *Rev. Mod. Phys.* **69**, 865–930 (1997).
- [9] Constantin, P. *et al.* Droplet breakup in a model of the hele-shaw cell. *Phys. Rev. E* **47**, 4169–4181 (1993).
- [10] Goldstein, R. E., Pesci, A. I. & Shelley, M. J. Attracting manifold for a viscous topology transition. *Phys. Rev. Lett.* **75**, 3665–3668 (1995).
- [11] Howell, P. D. The draining of a two-dimensional bubble. *J. Eng. Math.* **35**, 251–272 (1999).
- [12] Maxworthy, T. Bubble formation, motion and interaction in a hele-shaw cell. *J. Fluid Mech.* **173**, 95–114 (1986).
- [13] Kopf-Sill, A. R. & Homsy, G. M. Bubble motion in a hele-shaw cell. *Phys. Fluids* **31**, 18–26 (1988).
- [14] Maruvada, S. R. K. & Park, C.-W. Retarded motion of bubbles in hele-shaw cells. *Phys. Fluids* **8**, 3229–3233 (1996).
- [15] Shad, S., Salarieh, M., Maini, B. & Gates, I. D. The velocity and shape of convected elongated



- liquid drops in narrow gaps. *J. Petroleum Sci. Eng.* **72**, 67–77 (2010).
- [16] Aussillous, P. & Quéré, D. Bubbles creeping in a viscous liquid along a slightly inclined plane. *EPL (Europhysics Letters)* **59**, 370 (2002).
- [17] Reyssat, E. Drops and bubbles in wedges. *J. Fluid. Mech.* **748**, 641–662 (2014).
- [18] Dubois, C., Duchesne, A. & Caps, H. Between inertia and viscous effects: Sliding bubbles beneath an inclined plane. *EPL (Europhys. Lett.)* **115**, 44001 (2016).
- [19] Courbin, L. *et al.* Imbibition by polygonal spreading on microdecorated surfaces. *Nat. Mater.* **6**, 661–664 (2007).
- [20] Ishino, C., Reyssat, M., Reyssat, E., Okumura, K. & Quéré, D. Wicking within forests of micropillars. *Europhys. Lett.* **79**, 56005–(1–5) (2007).
- [21] Obara, N. & Okumura, K. Imbibition of a textured surface decorated by short pillars with rounded edges. *Phys. Rev. E* **86**, 020601(R) (2012).
- [22] Tani, M. *et al.* Capillary rise on legs of a small animal and on artificially textured surfaces mimicking them. *Plos One* **9**, e96813 (2014).
- [23] Tani, M., Kawano, R., Kamiya, K. & Okumura, K. Towards combinatorial mixing devices without any pumps by open-capillary channels: fundamentals and applications. *Sci. Rep.* **5**, 10263– (2015).
- [24] Gorce, J.-B., Hewitt, I. J. & Vella, D. Capillary imbibition into converging tubes: Beating washburnfs law and the optimal imbibition of liquids. *Langmuir* **32**, 1560–1567 (2016).
- [25] Cantat, I. *et al.* *Les mousses: structure et dynamique* (Belin, Paris, 2010).
- [26] Biance, A.-L., Cohen-Addad, S. & Höhler, R. Topological transition dynamics in a strained bubble cluster. *Soft Matter* **5**, 4672–4679 (2009).
- [27] Yazhgur, P. *et al.* How antifoams act: a microgravity study. *npj Microgravity* **1** (2015).
- [28] Denkov, N. D., Tcholakova, S., Golemanov, K., Ananthpadmanabhan, K. & Lips, A. The role of surfactant type and bubble surface mobility in foam rheology. *Soft Matter* **5**, 3389–3408 (2009).
- [29] Nordstrom, K. *et al.* Microfluidic rheology of soft colloids above and below jamming. *Phys. Rev. Lett.* **105**, 175701 (2010).
- [30] Seth, J., Mohan, L., Locatelli-Champagne, C., Cloitre, M. & Bonnecaze, R. A micromechanical model to predict the flow of soft particle glasses. *Nature Mater.* **10**, 838–843 (2011).
- [31] de Gennes, P.-G., Brochard-Wyart, F. & Quéré, D. *Gouttes, Bulles, Perles et Ondes, 2nd.*

- eds.* (Belin, Paris, 2005).
- [32] Landau, L. & Levich, B. *Physicochim. Acta. Physicochim (URSS)* **17**, 42 (1942).
  - [33] Derhaguin, B. *Physicochim. Acta. Physicochim (URSS)* **20**, 349 (1943).
  - [34] Park, C.-W. & Homsy, G. Two-phase displacement in hele shaw cells: theory. *J. Fluid Mech.* **139**, 291–308 (1984).
  - [35] Yahashi, M., Kimoto, N. & Okumura, K. Scaling crossover in thin-film drag dynamics of fluid drops in the hele-shaw cell. *Sci. Rep.* **6**, 31395 (2016).
  - [36] Takehara, Y. & Okumura, K. High-velocity drag friction in granular media near the jamming point. *Phys. Rev. Lett.* **112**, 148001 (2014).
  - [37] Okumura, K. Simple views on different problems in physics: from drag friction to tough biological materials. *Phil. Mag.* **96**, 828–841 (2016).
  - [38] Liu, A. J. & Nagel, S. R. Nonlinear dynamics: Jamming is not just cool any more. *Nature* **396**, 21–22 (1998).
  - [39] Bi, D., Zhang, J., Chakraborty, B. & Behringer, R. Jamming by shear. *Nature* **480**, 355–358 (2011).
  - [40] O’Hern, C., Langer, S., Liu, A. & Nagel, S. Random packings of frictionless particles. *Phys. Rev. Lett.* **88**, 75507 (2002).
  - [41] O’Hern, C., Silbert, L., Liu, A. & Nagel, S. Jamming at zero temperature and zero applied stress: The epitome of disorder. *Phys. Rev. E* **68**, 011306 (2003).
  - [42] Olsson, P. & Teitel, S. Critical scaling of shear viscosity at the jamming transition. *Phys. Rev. Lett.* **99**, 178001 (2007).
  - [43] Boyer, F., Guazzelli, E. & Pouliquen, O. Unifying suspension and granular rheology. *Phys. Rev. Lett.* **107**, 188301 (2011).
  - [44] Lerner, E., Düring, G. & Wyart, M. A unified framework for non-brownian suspension flows and soft amorphous solids. *Proc. Nat. Acad. Sci. (U.S.A.)* **109**, 4798–4803 (2012).
  - [45] Waitukaitis, S., Roth, L., Vitelli, V. & Jaeger, H. Dynamic jamming fronts. *EPL (Europhys. Lett.)* **102**, 44001 (2013).
  - [46] Tighe, B. P., Woldhuis, E., Remmers, J. J. C., van Saarloos, W. & van Hecke, M. Model for the scaling of stresses and fluctuations in flows near jamming. *Phys. Rev. Lett.* **105**, 088303 (2010).
  - [47] Hatano, T. Scaling properties of granular rheology near the jamming transition. *J. Phys. Soc.*

- Jpn.* **77**, 123002 (2008).
- [48] Otsuki, M. & Hayakawa, H. Universal scaling for the jamming transition. *Prog. Theor. Phys.* **121**, 647–655 (2009).
  - [49] Otsuki, M. & Hayakawa, H. Rheology of sheared granular particles near jamming transition. *Prog. Theor. Phys. Suppl.* **195**, 129–138 (2012).
  - [50] Clark, A. H., Kondic, L. & Behringer, R. P. Particle scale dynamics in granular impact. *Phys. Rev. Lett.* **109**, 238302 (2012).
  - [51] Goldman, D. I. & Umbanhowar, P. *Phys. Rev. E* **77**, 021308– (2008).
  - [52] Katsuragi, H. & Durian, D. J. *Nature Phys.* **3**, 420– (2007).
  - [53] Wieghardt, K. *Annu. Rev. Fluid. Mech.* **7**, 89– (1975).
  - [54] Albert, R., Pfeifer, M., Barabási, A.-L. & Schiffer, P. Slow drag in a granular medium. *Phys. Rev. Lett.* **82**, 205 (1999).
  - [55] Hartley, R. R. & Behringer, R. P. *Nature* **421**, 928– (2003).
  - [56] Chehata, D., Zenit, R. & Wassgren, C. R. *Phys. Fluids* **15**, 1622– (2003).
  - [57] Hastings, M. B., Olson Reichhardt, C. J. & Reichhardt, C. Depinning by fracture in a glassy background. *Phys. Rev. Lett.* **90**, 098302 (2003).
  - [58] Drocco, J. A., Hastings, M. B., Reichhardt, C. J. O. & Reichhardt, C. *Phys. Rev. Lett.* **95**, 088001– (2005).
  - [59] Costantino, D. J. *et al.* Starting to move through a granular medium. *Phys. Rev. Lett.* **101**, 108001 (2008).
  - [60] Candelier, R. & Dauchot, O. Creep motion of an intruder within a granular glass close to jamming. *Phys. Rev. Lett.* **103**, 128001 (2009).
  - [61] Kolb, E., Cixous, P., Gaudouen, N. & Darnige, T. Rigid intruder inside a two-dimensional dense granular flow: Drag force and cavity formation. *Phys. Rev. E* **87**, 032207 (2013).
  - [62] Takada, S. & Hayakawa, H. Drag law of two dimensional granular fluids. *J. Eng. Mech.* doi: 10.1061/(ASCE)EM.1943-7889.0001054 (2016).
  - [63] Seguin, A., Lefebvre-Lepot, A., Faure, S. & Gondret, P. Clustering and flow around a sphere moving into a grain cloud. *Eur. Phys. J. E* **39**, 63– (2016).
  - [64] Aarts, D. G. A. L., Lekkerkerker, H. N. W., Guo, H., Wegdam, G. H. & Bonn, D. Hydrodynamics of droplet coalescence. *Phys. Rev. Lett.* **95**, 164503 (2005).
  - [65] Eggers, J., Lister, J. & Stone, H. Coalescence of liquid drops. *J. Fluid Mech.* **401**, 293–310

- (1999).
- [66] Burton, J. C. & Taborek, P. Role of dimensionality and axisymmetry in fluid pinch-off and coalescence. *Phys. Rev. Lett.* **98**, 224502 (2007).
  - [67] Paulsen, J. D., Carmigniani, R., Kannan, A., Burton, J. C. & Nagel, S. R. Coalescence of bubbles and drops in an outer fluid. *Nature Commun.* **5** (2014).
  - [68] Yokota, M. & Okumura, K. Dimensional crossover in the coalescence dynamics of viscous drops confined in between two plates. *Proc. Nat. Acad. Sci. (U.S.A.)* **108**, 6395–6398; In this issue, PNAS, 108 (2011) 6337. (2011).
  - [69] Charles, G. E. & Mason, S. G. The mechanism of partial coalescence of liquid drops at liquid/liquid interfaces. *Journal of Colloid Science* **15**, 105–122 (1960).
  - [70] Blanchette, F. & Bigioni, T. P. Partial coalescence of drops at liquid interfaces. *Nature Physics* **2**, 254–257 (2006).
  - [71] Pucci, G., Harris, D. M. & Bush, J. W. Partial coalescence of soap bubbles. *Phys. Fluids* **27**, 061704 (2015).
  - [72] Oron, A., Davis, S. H. & Bankoff, S. G. Long-scale evolution of thin liquid films. *Rev. Mod. Phys.* **69**, 931–980 (1997).
  - [73] Reiter, G. *et al.* Residual stresses in thin polymer films cause rupture and dominate early stages of dewetting. *Nature Mater.* **4**, 754–758 (2005).
  - [74] Damman, P. *et al.* Relaxation of residual stress and reentanglement of polymers in spin-coated films. *Phys. Rev. Lett.* **99**, 036101 (2007).
  - [75] Culick, F. Comments on a ruptured soap film. *J. Appl. Phys.* **31**, 1128–1129 (1960).
  - [76] McEntee, W. R. & Mysels, K. J. Bursting of soap films. i. an experimental study. *J. Phys. Chem.* **73**, 3018–3028 (1969).
  - [77] Frankel, S. & Mysels, K. J. Bursting of soap films. ii. theoretical considerations. *J. Phys. Chem.* **73**, 3028–3038 (1969).
  - [78] Reyssat, E. & Quere, D. Bursting of a fluid film in a viscous environment. *EPL (Europhys. Lett.)* **76**, 236 (2006).
  - [79] Redon, C., Brochard-Wyart, F. & Rondelez, F. Dynamics of dewetting. *Phys. Rev. Lett.* **66**, 715–718 (1991).
  - [80] Debrégeas, G., Martin, P. & Brochard-Wyart, F. Viscous bursting of suspended films. *Phys. Rev. Lett.* **75**, 3886 (1995).

- [81] Eri, A. & Okumura, K. Bursting of a thin film in a confined geometry: Rimless and constant-velocity dewetting. *Phys. Rev. E* **82**, 030601(R) (2010).
- [82] Squires, T. M. & Quake, S. R. Microfluidics: Fluid physics at the nanoliter scale. *Rev. Mod. Phys.* **77**, 977 (2005).
- [83] Weaire, D. & Hutzler, S. *The Physics of Foams* (Clarendon Press, Oxford, 1999).

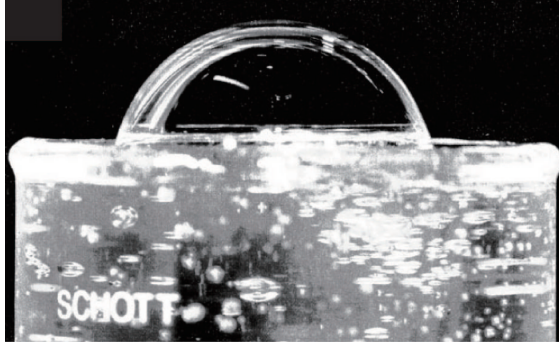


FIG. 1: Hemispherical air bubble formed at a liquid-air interface in a ultra-viscous liquid. Taken from [1].

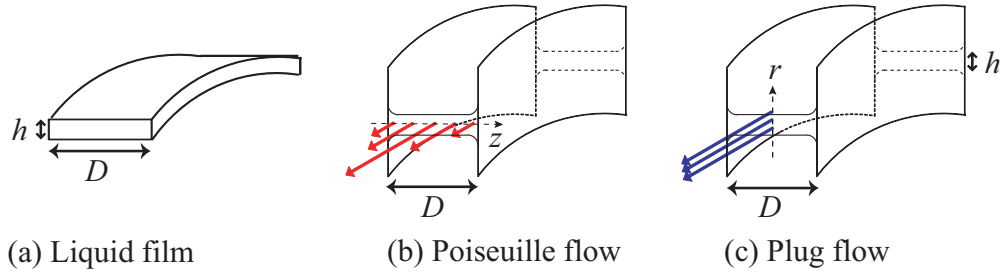


FIG. 2: (a) A part of the liquid film sandwiched by two cell plates separated by the distance  $D$ . In the direction of cell thickness (i.e., the  $z$  direction), the flow changes as in (b). In the direction of film thickness (i.e., in the  $r$  direction), the flow does not change as in (c).

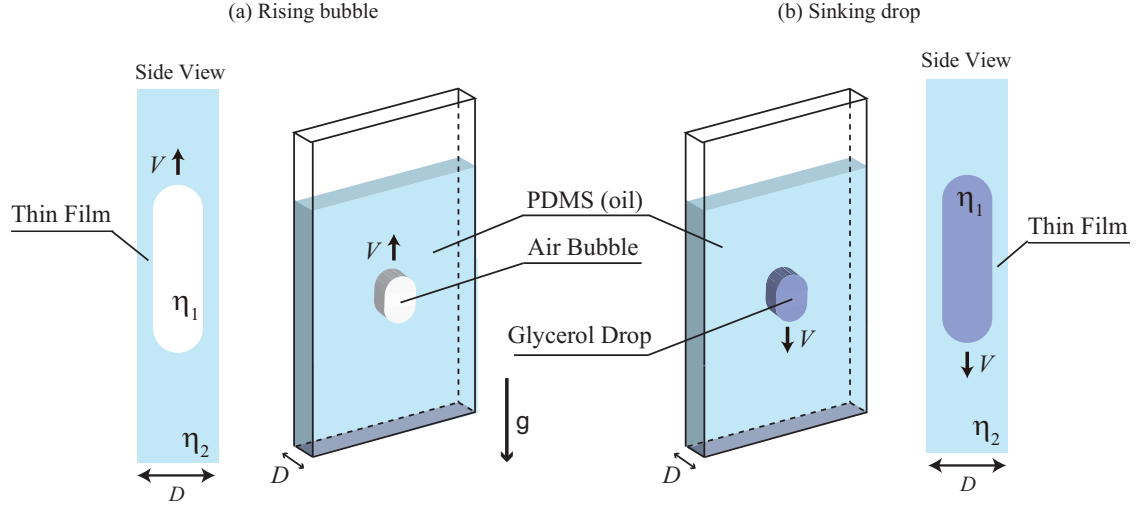


FIG. 3: Illustrations of experiments for a rising bubble (a) and for a sinking drop (b). The Hele-Shaw cell is made up of transparent acrylic plates. The cell thickness  $D$  is a few millimeters and the size of the bubble or drop is about one centimeter. The width and height of the cell are much larger than the size of the drop. Side views show that the existence of liquid thin films between the fluid drop (the bubble or liquid drop) and the cell walls.  $\eta_1$  and  $\eta_2$  respectively denote viscosities of the fluid drop and the liquid surrounding the fluid drop.

### Rising Bubble and Sinking Drops

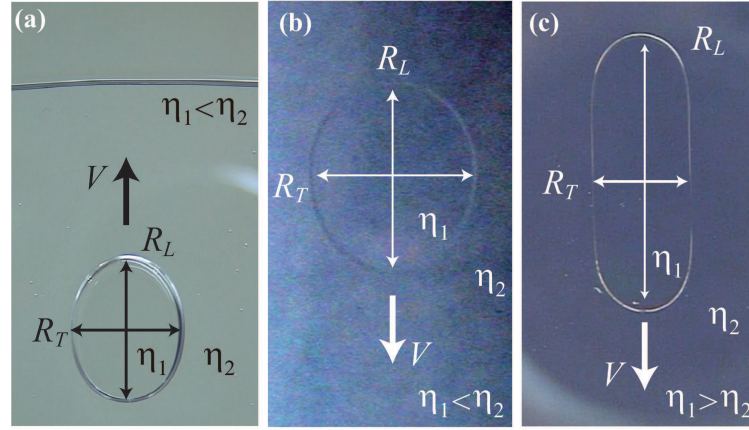


FIG. 4: Moving fluid drops in a Hele-Shaw cell. Here, the viscosity of the fluid drop (bubble or liquid drop) and the surrounding fluid are denoted  $\eta_1$  and  $\eta_2$ , respectively. (a) The rising bubble ("air drop") is slightly deformed from a circle and characterized by the longitudinal and transverse diameters,  $R_L$  and  $R_T$ , respectively, as indicated in the photograph. (b) A glycerol drop surrounded by a more viscous oil [as in (a)] is sinking in the cell. The fluid drop shape is very similar to that in (a). (c) A glycerol drop surrounded by a less viscous oil [different from (a) and (b)] is sinking in the cell. Compared with (a) and (b), the elongation is significant. Figures are adapted from [3].



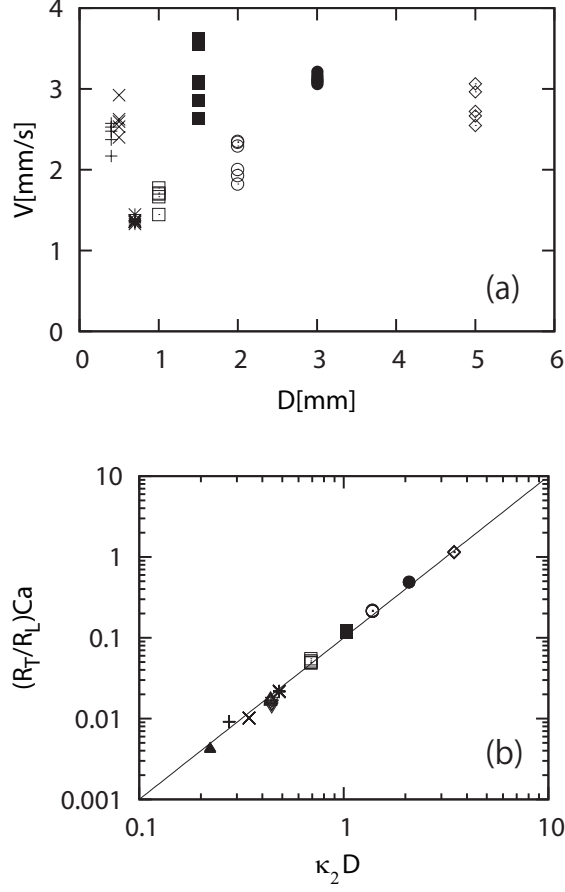


FIG. 5: (a)  $V$  vs  $D$  for different  $R_T, R_L$ , and  $\nu_2 = \eta_2/\rho_2$ . The 8 symbols  $+$ ,  $\times$ ,  $*$ ,  $\square$ ,  $\blacksquare$ ,  $\circ$ ,  $\bullet$ , and  $\diamond$  correspond to  $(D \text{ [mm]}, \nu_2 \text{ [cS]}) = (0.4, 100), (0.5, 100), (0.7, 500), (1.0, 1000), (1.5, 1000), (2.0, 3000), (3.0, 5000), \text{ and } (5.0, 10000)$ , respectively. (b) Plot in (a) replotted with the two axes, the renormalized velocity  $(R_T/R_L)Ca$  and the renormalized cell thickness  $\kappa_2 D$ , demonstrating a clear data collapse by virtue of the theory. Figures are reproduced from [3].

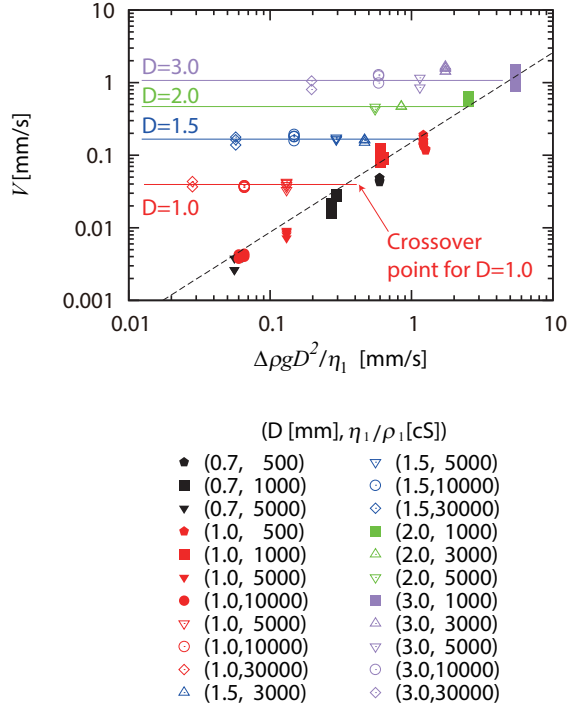


FIG. 6:  $V$  vs.  $\Delta\rho g D^2 / \eta_1$ . Data represented by the filled symbols are well on the dashed line, confirming the scaling law given in Eq. (13) for  $\eta_2 < \eta_1$ . The data including the data represented by the open symbols are further discussed in Fig. 7. Figures are adapted from Ref. [35].

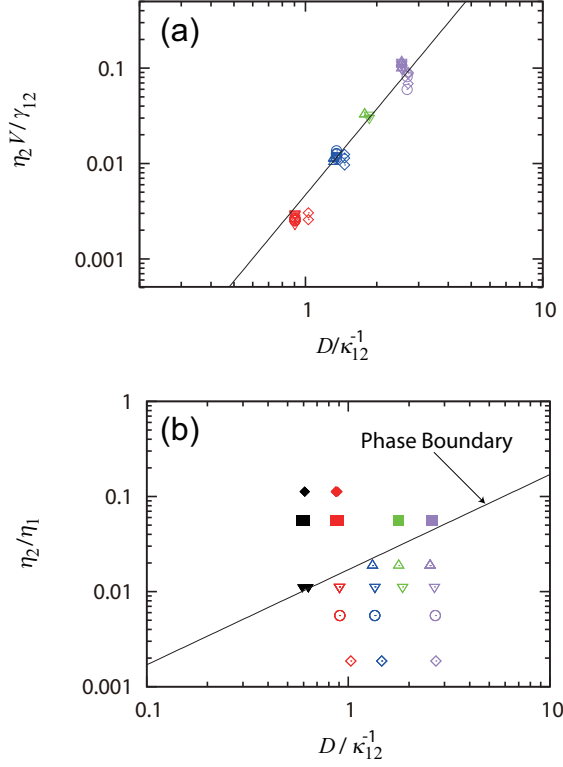


FIG. 7: (a)  $\eta_1 V / \gamma_{12}$  vs.  $D / \kappa_{12}^{-1}$  on a log-log scale. Data represented by the open symbols are well on the line with slope 3, confirming the scaling law given in Eq. (14) for  $D > \kappa_{12}^{-1}$ . (b)  $\eta_2 / \eta_1$  vs.  $D / \kappa_{12}^{-1}$ , confirming the crossover condition given in Eq. (19); the line representing phase boundary separates the data represented by the filled symbols from those by the open symbols. The symbols are the same ones with those used in Fig. 6. Figures are adapted from Ref. [35].

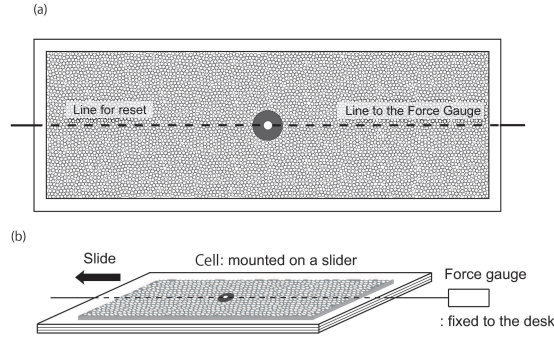


FIG. 8: Setup for the experiment for granular drag friction. (a) View of the cell from above. (b) Slanted view of the setup. One layer of granular particles of average diameter  $d = 2$  mm are packed in a two-dimensional cell made of transparent acrylic plates. The diameter  $2R$  of the obstacle is about ten times larger than  $d$ . Reproduced from [36].

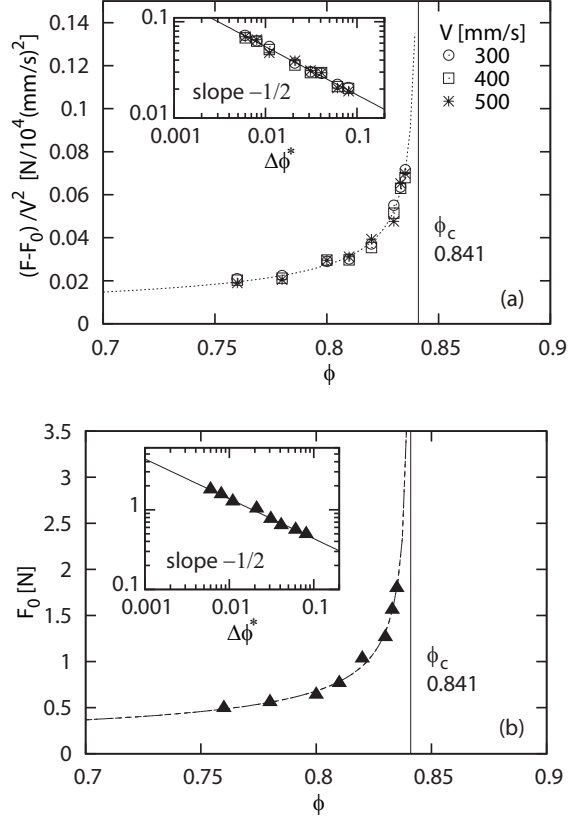


FIG. 9: Divergence of the dynamic (a) and static (b) components of the granular drag force at the jamming point  $\phi = \phi_c$ . Reproduced from [36].

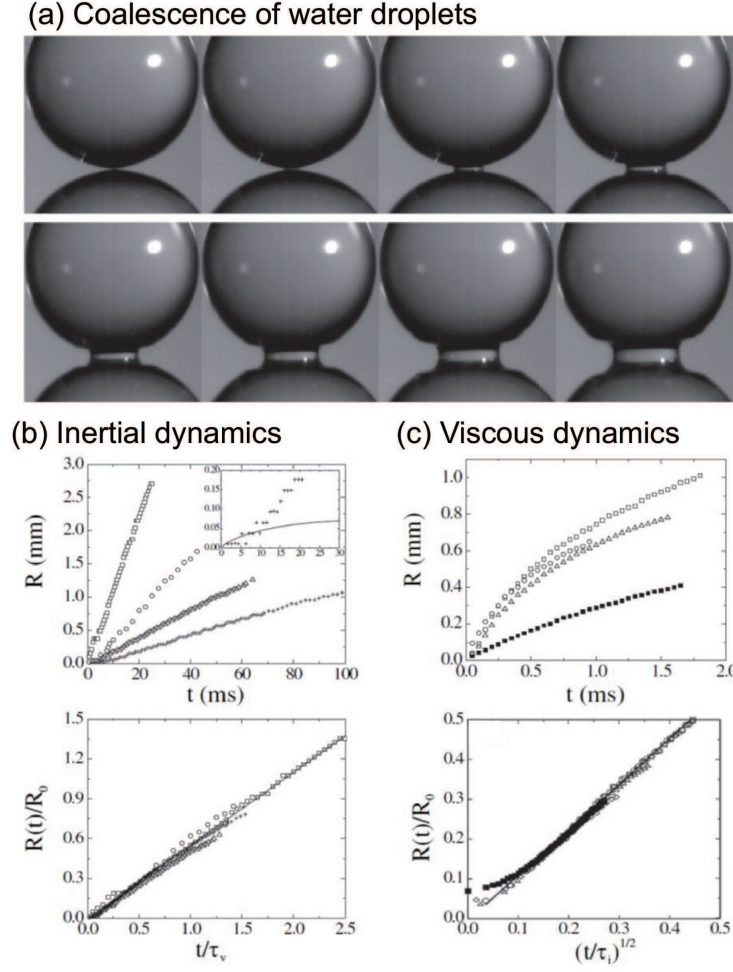
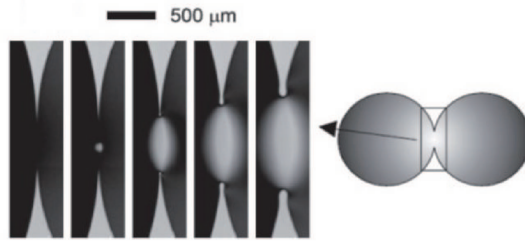


FIG. 10: Three dimensional coalescence. (a) Coalescence of water droplets captured by a high-speed camera (11,200 frame per second). (b) Inertial dynamics. The raw data in the top panel are collapse onto a single master curve in the bottom, by virtue of rescaling of both axes according to Eq. (22). (c) Viscous dynamics. Another example of data collapse is shown, confirming Eq. (22). Taken from Ref. [64]©2005 with permission from APS.

(a) Purely two-dimensional coalescence



(b) Scaling crossover

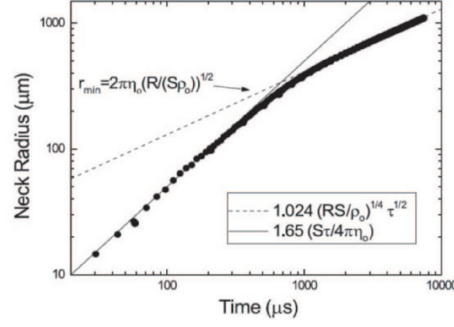


FIG. 11: Purely two-dimensional coalescence. (a) Coalescence of dodecane droplets floating on water captured by a high-speed camera (the time interval between frames is  $748 \mu\text{s}$ ). The gravity points in the direction perpendicular to the paper. The right illustration is the overview of two thin “liquid lens” floating on the horizontal surface of a bath of water, which are represented by two circles contacting with each other at the center. In the left, magnified snapshots of the central part are arranged in time sequence (from left to right) showing the neck growth with time. (b) Scaling crossover between the viscous and inertial regimes, confirming Eq. (22). Taken from Ref. [66]©2007 with permission from APS.

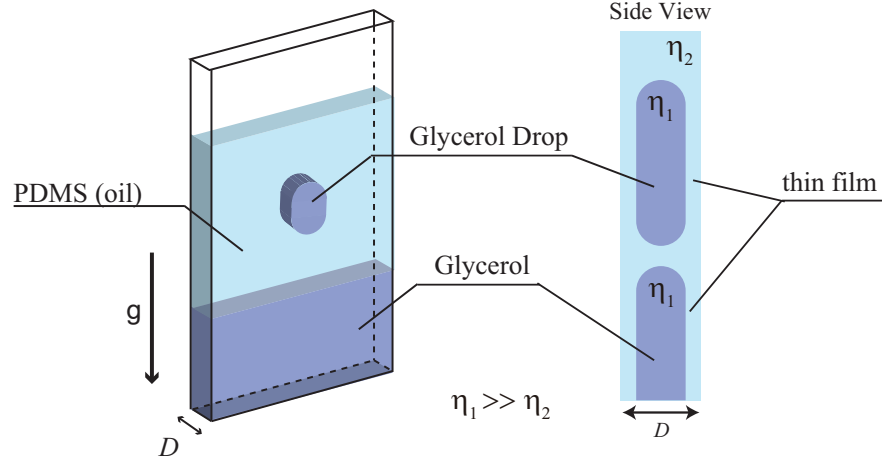


FIG. 12: Experimental setup to observe drop coalescence in a Hele-Shaw cell. The side view shows that the existence of liquid thin films between the drop (or the lower bath of the same liquid) and the cell walls.  $\eta_1$  and  $\eta_2$  respectively denote viscosities of the liquid drop and the liquid surrounding the liquid drop. The viscosity of the liquid in the lower bath phase is also  $\eta_1$ .

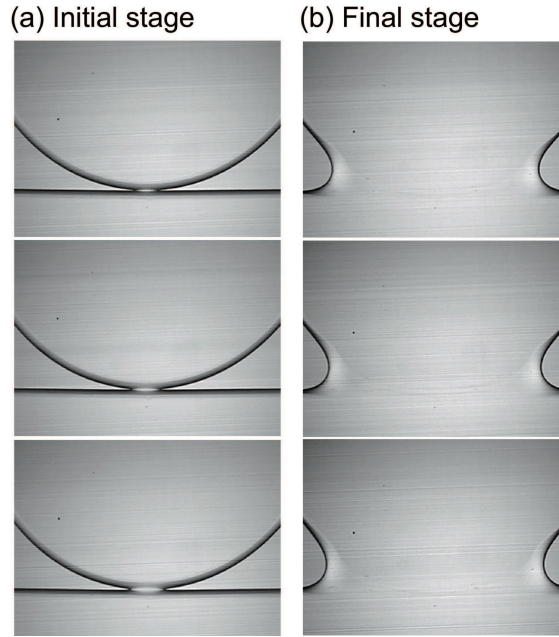


FIG. 13: Coalescence in a Hele-Shaw cell at short times (a) and at large times (a). The time intervals between adjacent shots in (a) and (b) are 4 ms and 40 ms, respectively. Adapted from [68].

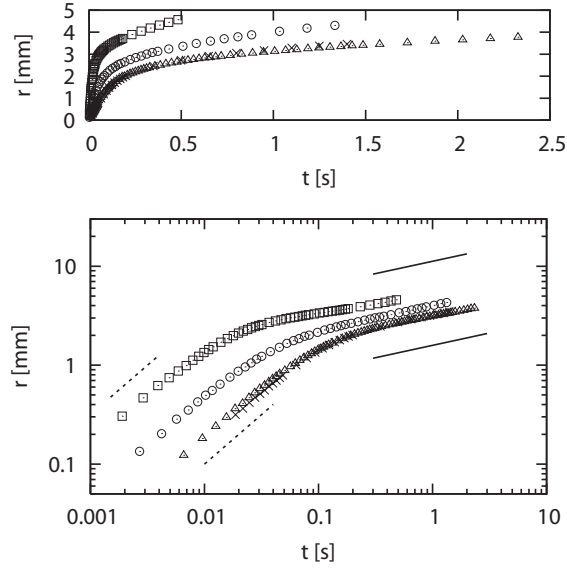


FIG. 14: Neck size  $r$  vs. time  $t$  for different parameters. The viscosity  $\eta_1$  [mPa·s] of the drop, cell thickness  $D$  [mm], and radius of the droplet  $R$  [mm] for each symbol are given as follows.  $\square$ : 62.9, 0.7, 5.62.  $\circ$ : 289, 0.7, 5.56.  $\triangle$ : 888, 1.0, 4.13.  $\times$ : 964, 1.0, 4.32. (a) The raw data. (b) The same data on a log-log scale, showing a clear scaling crossover. The slopes that represent the initial and final dynamics are 1 and 1/4, respectively. Adapted from [68].



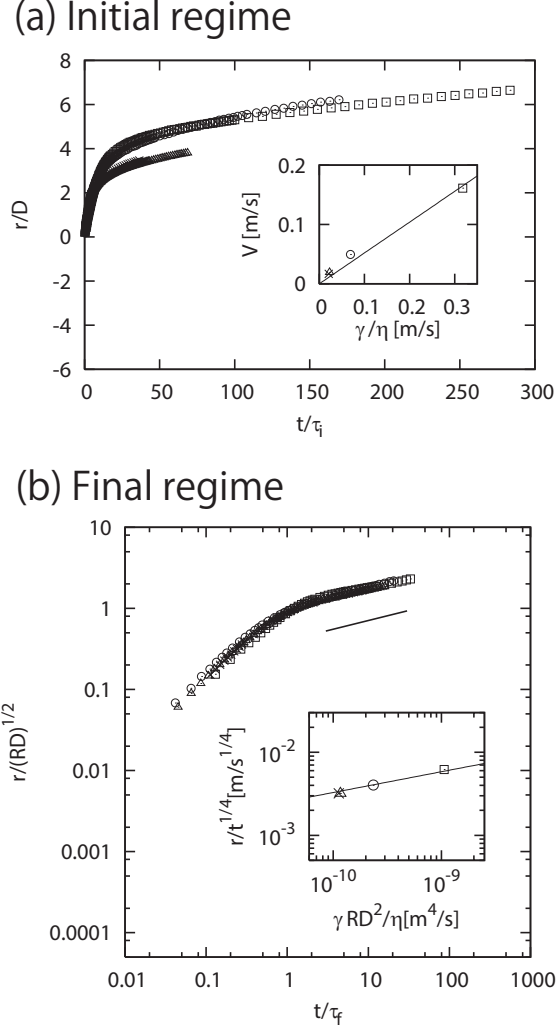


FIG. 15: Confirmation of the dimensional crossover expressed in Eqs. (23) and (24). (a) Initial regime. (b) Final regime. In the main plots, data collapses are shown for each regime. The insets show qualitative comparison of theory with experiment. In the plots,  $\tau_I$  and  $\tau_F$  in Eqs. (23) and (24) are expressed as  $\tau_i$  and  $\tau_f$ , respectively. In addition,  $\gamma_{12}$  and  $\eta_1$  are expressed by  $\gamma$  and  $\eta$ , respectively. Adapted from [68].

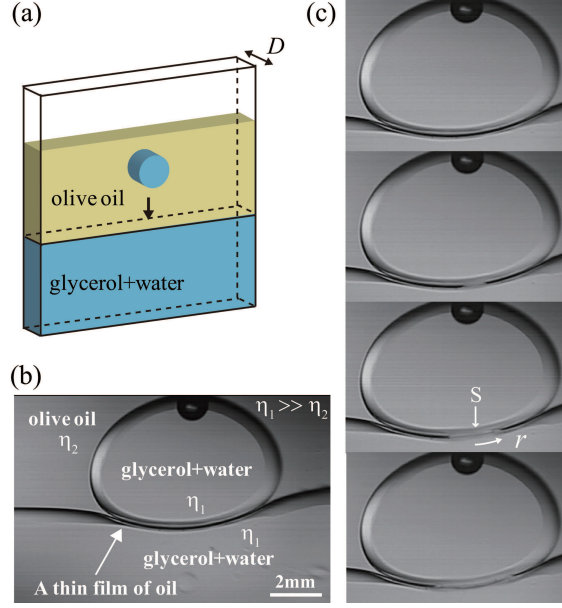


FIG. 16: (a) Illustration of the experiment. (b) A glycerol droplet sitting at the oil-glycerol interface where a thin oil film underneath the droplet disallows coalescence typically for a few minutes. The white bar stands for the cell thickness  $D$  ( $= 2$  mm). (c) The dynamics of coalescence: bursting of a thin film of oil between the droplet and the bath. The snapshots are separated by  $15/8000$  seconds. The length  $r$  stands for the distance between the bursting tip and the point (indicated as  $S$ ) where the bursting started.